https://doi.org/10.5194/egusphere-2026-1855
Preprint. Discussion started: 17 April 2026
© Author(s) 2026. CC BY 4.0 License.

Quantitative insights into regime-dependent aerosol pH variability in an ammonia-rich urban atmosphere from explainable machine learning

Jing Duan[1,†], Ting Wang[1,†], Ru-Jin Huang[1,2,3*], Jingye Ren[1], Haobin Zhong[4], Wei Xu[5], Chunshui Lin[1], Yanan Zhan[1,2], Huabin Huang[6], Yongjie Li[7]

[1]State Key Laboratory of Loess Science, Institute of Earth Environment, Chinese Academy of Sciences, Xi'an 710061, China

[2]Institute of Global Environmental Change, Xi'an Jiaotong University, Xi'an 710049, China

[3]University of Chinese Academy of Sciences, Beijing 100049, China

[4]School of Advanced Materials Engineering, Jiaxing Nanhu University, Jiaxing, 314001, China

[5]State Key Laboratory of Advanced Environmental Technology, Institute of Urban Environment, Chinese Academy of Sciences, Xiamen, China

[6]College of Environment and Public Health, Xiamen Huaxia University, Xiamen 361024, China

[7]Department of Civil and Environmental Engineering, Faculty of Science and Technology, University of Macau, Taipa, Macau SAR 999078, China

Correspondence to: Ru-Jin Huang (rujin.huang@ieecas.cn)

†Contributed equally to this study

Abstract

Aerosol acidity (pH) plays a crucial role in atmospheric chemistry. Meteorological conditions and chemical properties jointly contribute to pH variation, yet their behavior differs across environmental regimes and remain incompletely understood. Here, we integrate machine learning with interpretable model analyses, field observations, and thermodynamic modeling to quantitatively assess the relative contributions and associations of key factors to aerosol pH variability in an ammonia-rich urban atmosphere. Temperature exhibits a strong negative contribution to pH variation, with an average decrease of ~0.6 units per 10 °C increase. Excess ammonia, nitrate-to-sulfate mass ratio (N/S), and PM_1 mass loading are positively associated with pH, showing stronger sensitivities at lower values and diminishing responses at higher levels. In contrast, the contribution of relative humidity (RH) depends strongly on its

https://doi.org/10.5194/egusphere-2026-1855
Preprint. Discussion started: 17 April 2026
© Author(s) 2026. CC BY 4.0 License.

interactions with temperature, aerosol composition, and mass loading, resulting in pronounced regime-dependent reversals. Higher RH is associated with enhanced aerosol acidity under low-temperature (< 15 °C), nitrate-dominant (N/S > 1.25), or high-mass (PM_1 > 50 μg m^{-3}) conditions, whereas the opposite tendency occurs under warmer, sulfate-dominant, or low-mass regimes. This study provides new quantitative insights into the coupled meteorological and chemical modulation of pH and highlights the importance of multifactor interactions in understanding aerosol acidity variability in real-world atmospheres.

1. Introduction

Aerosol acidity (pH) critically modulates atmospheric multiphase processes, influencing gas–particle partitioning (Guo et al., 2016; Guo et al., 2017), secondary aerosol formation (Shi et al., 2019; Yang et al., 2022), pollutant transformation (Cao et al., 2020; Fu et al., 2022), and metal solubility (Tao and Murphy, 2019; Giorio et al., 2022), with important implications for air quality, climate, and human health (Mo et al., 2017; Myriokefalitakis et al., 2018; Su et al., 2020; Tilgner et al., 2021; Wei et al., 2023; Xie et al., 2023). Due to challenges in direct measurements, aerosol pH is commonly derived from thermodynamic equilibrium models such as ISORROPIA II and E-AIM, which estimate pH from observed chemical compositions and meteorological parameters (Clegg et al., 2001; Fountoukis and Nenes, 2007; Hennigan et al., 2015). Using such model-derived calculations, previous studies have reported globally variable aerosol acidity (Guo et al., 2016; Liu et al., 2017; Sharma et al., 2022). In China, aerosols generally exhibit higher pH relative to the United States and Europe, owing to its rich ammonia emission, and show distinct north–south gradients influenced by regional emissions and meteorology (Ding et al., 2019; Wang et al., 2020; Zhang et al., 2021).

Driving factors of aerosol pH in China's ammonia-rich environment have been explored in recent years using sensitivity analyses, yet a comprehensive understanding remains incomplete. For instance, Ding et al. (2019) identified sulfate, total ammonia, and temperature as common drivers of pH variations, with nitrate exerting less influence. In contrast, Xie et al. (2020) suggested that increases in the nitrate fraction, rather than ammonia, can elevate pH. Proposing a multiphase buffer theory, Zheng et al. (2020) showed that aerosol water content and particle mass may outweigh chemical composition in controlling pH in ammonia-rich regions. Long-

https://doi.org/10.5194/egusphere-2026-1855
Preprint. Discussion started: 17 April 2026
© Author(s) 2026. CC BY 4.0 License.

term observations, however, pointed to meteorology (temperature and relative humidity) as the dominant factors for seasonal and diurnal pH variability (Zhou et al., 2022; Duan et al., 2025). These discrepancies indicate that the coupled contributions of chemical and meteorological factors to aerosol pH variation are complex and strongly regime-dependent, warranting further comprehensive investigation. Importantly, decomposition of pH variation has primarily focused on the linear additive contributions of individual factors, relying on thermodynamic sensitivity tests and simple quantitative frameworks (Tao and Murphy, 2021; Wang et al., 2022; Zhou et al., 2022), while providing limited insight into potential nonlinear interactions among chemical and meteorological parameters that may jointly shape pH dynamics. Addressing this gap is therefore essential for achieving a more mechanistic understanding of aerosol acidity under different atmospheric environments.

Machine learning (ML) methods, combined with interpretable techniques such as Shapley Additive Explanations (SHAP), have emerged as powerful tools for capturing nonlinear relationships and high-dimensional dependencies in atmospheric studies (Grange et al., 2018; Hou et al., 2022; Song et al., 2022). SHAP provides a unified framework for quantifying the marginal contributions of individual predictors and their nonlinear interactions (Lundberg et al., 2020), making it particularly suitable for assessing how chemical composition and meteorological conditions jointly relate to atmospheric processes (Hou et al., 2022; Dai et al., 2023; Peng et al., 2023). In this study, we integrate thermodynamic model calculations with a SHAP-based ML framework to provide quantitative insights into the relative contributions of key factors to aerosol pH variability in an ammonia-rich atmosphere. Based on a full year of continuous observations from a northern Chinese city, this approach characterizes how chemical composition and meteorological conditions are jointly associated with aerosol acidity, quantifies their statistical interactions across diverse environmental regimes, and advances understanding of the processes underlying aerosol pH.

2. Materials and methods

2.1 Field observations

Continuous measurements were conducted from 21 December 2014 to 31 December 2015 at an urban site located on the rooftop of the National Center for Nanoscience in Beijing (39.99°N,

https://doi.org/10.5194/egusphere-2026-1855
Preprint. Discussion started: 17 April 2026
© Author(s) 2026. CC BY 4.0 License.

116.32°E). Non-refractory PM_1 species, including organics (OA), sulfate (SO_4^{2-}), nitrate (NO_3^-), ammonium (NH_4^+), and chloride (Cl^-), were quantified using an Aerodyne quadrupole aerosol chemical speciation monitor (Q-ACSM) (Ng et al., 2011). Gaseous ammonia (NH_3) was measured with a Picarro G2103 analyzer (Maasikmets et al., 2015). Meteorological parameters, including temperature and relative humidity (RH), were simultaneously recorded using an automatic weather station (MAWS201, Vaisala, Finland) (Wang et al., 2017). Details on sampling and instrumentation are provided in Text S1.

2.2 Aerosol pH calculation

Aerosol pH was estimated using the ISORROPIA II thermodynamic model (Fountoukis and Nenes, 2007). The input dataset included the measured concentrations of SO_4^{2-}, NO_3^-, Cl^-, and total ammonia (NH_3+NH_4^+), together with meteorological parameters (RH and temperature). The model outputs, including hydronium ion concentration (H_{air}^+) and aerosol liquid water content (ALWC), were subsequently adopted to calculate PM_1 pH according to Eq (1) (Guo et al., 2015):

$$pH = -\mathrm{Log}_{10}\gamma_{H^+}H_{aq}^+ = -\mathrm{Log}_{10}\frac{1000\gamma_{H^+}H_{air}^+}{ALWC_i+ALWC_o} \cong -\mathrm{Log}_{10}\frac{1000\gamma_{H^+}H_{air}^+}{ALWC_i} \quad (1)$$

where γ_{H^+} is the activity coefficient of hydronium ion (assumed to be unity), H_{aq}^+ (mol L^{-1}) is the concentration of hydronium ion in particle liquid water, H_{air}^+ (μg m^{-3}) is the mass concentration of hydronium ion in air, and $ALWC_i$ and $ALWC_o$ (μg m^{-3}) is the water concentration of bulk particle related to inorganic and organic species, respectively. Since the pH predictions were insensitive to $ALWC_o$ according to previous studies (Battaglia Jr et al., 2019; Guo et al., 2015; Ding et al., 2019), we only consider the portion of $ALWC_i$ in pH calculation.

Previous studies have shown that pH predictions from thermodynamic models can exhibit substantial biases when operated in the "reverse" mode (Hennigan et al., 2015; Song et al., 2018). Meanwhile, H^+ is inherently unstable under efflorescent particle conditions (Hennigan et al., 2015). To minimize these uncertainties, we ran ISORROPIA II in "forward" mode and "metastable" state, assuming fully deliquesced aerosols without solid formation. Furthermore, only data with RH > 30% were included to avoid unrealistic pH values arising from

https://doi.org/10.5194/egusphere-2026-1855
Preprint. Discussion started: 17 April 2026
© Author(s) 2026. CC BY 4.0 License.

misestimated ALWC at low RH, as noted in previous studies (Liu et al., 2017; Ding et al., 2019; Xie et al., 2020).

The accuracy of the thermodynamic simulation and the resulting pH prediction was evaluated by comparing the predicted and observed NH_3/NH_4^+ partitioning (Guo et al., 2016). As shown in Fig. S1, the modeled values agree well with the measurements (R^2 = 0.82-0.96, slope = 0.80-1.07), indicating that the performance of the ISORROPIA II model is satisfactory for this study.

2.3 Explainable machine learning model and interpretation

An explainable machine-learning model based on the extreme gradient boosting (XGBoost) algorithm was developed (Gui et al., 2020; Peng et al., 2023; Cai et al., 2025). The input features included chemical indicators such as excess ammonia (Excess NHx, calculated as described in Text S2), nitrate-to-sulfate mass ratio (N/S ratio), and PM_1 mass loading, together with meteorological parameters (temperature and RH). Aerosol pH calculated using ISORROPIA II served as the target variable. These features were selected because they collectively capture key meteorological and chemical characteristics potentially influencing aerosol pH, according to previous studies (Liu et al., 2017; Zheng et al., 2020; Zhou et al., 2022). The dataset was randomly divided into training (70%) and testing (30%) subsets. A 10-fold cross-validation procedure, repeated five times, was applied to ensure robust generalization and reduce overfitting (Qin et al., 2022; Peng et al., 2023). Model performance was evaluated using the root mean square error (RMSE, 0.12), mean absolute error (MAE, 0.08), and coefficient of determination (R^2 = 0.98; Fig. S2).

The Shapley additive explanations (SHAP) algorithm (Lundberg et al., 2020) was employed to interpret model outputs and quantify the relative importance of each predictor (the XGBoost–SHAP framework). SHAP assigns each input variable a contribution to the model output, capturing potential nonlinear effects. For each sample, the predicted value can be expressed as:

$$f(x_i)=\phi_0(f,x)+\sum_{i=1}^{M}\phi_j(f,x_i) \qquad (2)$$

where $f(x_i)$ is the predicted value for sample (x_i) with M features, $\phi_0(f, x)$ is the base value (expected output), and $\phi_j(f, x_i)$ is the SHAP value of feature j (Lundberg et al., 2020). In addition

https://doi.org/10.5194/egusphere-2026-1855
Preprint. Discussion started: 17 April 2026
© Author(s) 2026. CC BY 4.0 License.

to quantifying the marginal contribution of individual features, the SHAP framework was extended to compute pairwise interaction values using the Shapley interaction index from cooperative game theory (Lundberg et al., 2020). This approach decomposes each prediction into nonlinear main effects and interaction effects, providing more informative local explanations for individual predictions (Hou et al., 2022; Qi et al., 2025). By isolating these terms at the sample level, SHAP interaction analysis characterizes how combinations of predictors jointly influence model outputs, patterns that may not be captured by marginal SHAP values alone.

Centered individual conditional expectation (c-ICE) plots were also employed to examine nonlinear effects and feature interactions. Individual conditional expectation (ICE) curves describe how model predictions change as a single feature varies while all other features are held fixed, thereby preserving sample-specific trajectories and capturing the heterogeneity of feature effects across observations (Wei et al., 2022). However, the interpretation of ICE curves can be hindered by substantial vertical offsets among individual curves. To address this, c-ICE curves are constructed by centering each ICE curve at a reference point, effectively removing vertical shifts and highlighting the variation in predictions attributable to the feature itself (Yang et al., 2023; Yang et al., 2024). Divergences or non-parallel patterns among c-ICE curves indicate that the effect of a given feature depends on the values of other predictors, providing visual evidence of feature interactions at the sample-specific level.

3. Results and discussion

3.1 Relative importance of key factors for overall pH variability

Time series of meteorological and chemical measurements, together with ISORROPIA-derived pH and ALWC, are shown in Fig. 1. Aerosol pH ranged from 0.8 to 6.7 (average of 3.8), comparable to previous observations in North China (Ding et al., 2019; Xie et al., 2020; Wei et al., 2023), and displayed pronounced seasonal and synoptic variability. Excess NHx remained positive, indicating strongly ammonia-rich conditions (Song et al., 2018), while the N/S ratio spanned from sulfate-dominant to nitrate-dominant states. The temporal variability in chemical composition and meteorology provides a representative dataset for quantifying their relative contributions to aerosol acidity variation across diverse environmental conditions.

https://doi.org/10.5194/egusphere-2026-1855
Preprint. Discussion started: 17 April 2026
© Author(s) 2026. CC BY 4.0 License.

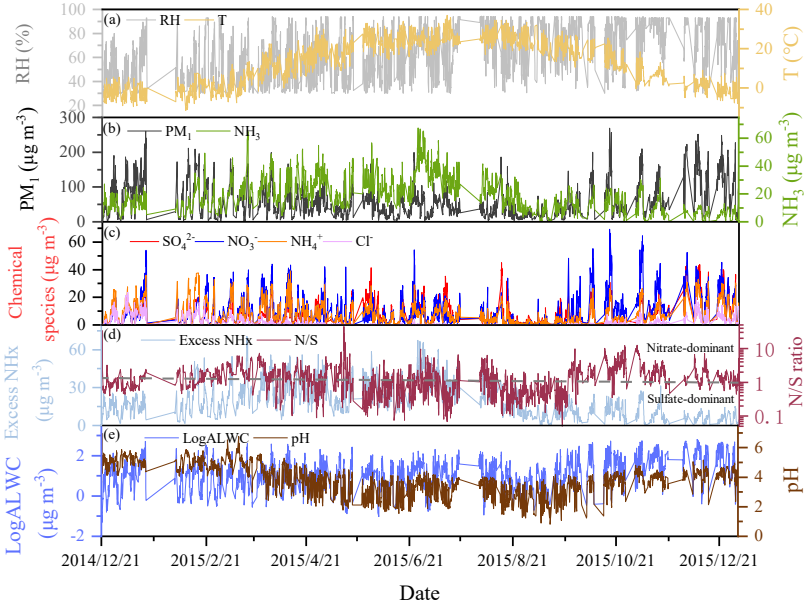

Figure 1. Time series of meteorological and chemical measurements and derived model variables during the sampling period. Panels show (a) temperature and relative humidity (RH), (b) mass concentrations of PM_1 and gaseous NH_3, (c) inorganic species including SO_4^{2-}, NO_3^-, NH_4^+, and Cl^-, (d) Excess NHx and the nitrate-to-sulfate mass ratio (N/S ratio), and (e) aerosol pH and aerosol liquid water content (ALWC) calculated by ISORROPIA II.

The mean absolute SHAP values provide a global ranking of predictors contributing to aerosol pH variability across the observation period (Fig. S3). Temperature emerges as the most significant factor, followed by Excess NHx, N/S ratio, RH, and PM_1 mass loading. The dominant role of temperature in explaining the overall pH variability is consistent with previous thermodynamic sensitivity analyses (Jia et al., 2020; Tao and Murphy, 2021). Examining each predictor in detail (Fig. 2), SHAP values show a strong, monotonic negative contribution of temperature, with low-temperature conditions corresponding to higher pH. This pattern aligns with thermodynamic predictions, in which lower temperatures favor ammonia partitioning into the particle phase and higher aerosol liquid water, both likely elevate pH (Ding et al., 2019; Jia et al., 2020). Both higher Excess NH_x and elevated N/S ratio correspond to positive SHAP

https://doi.org/10.5194/egusphere-2026-1855
Preprint. Discussion started: 17 April 2026
© Author(s) 2026. CC BY 4.0 License.

contributions, consistent with previous thermodynamic analyses suggesting more ammonia-rich and nitrate-rich conditions generally enhance aerosol neutralization and shift pH upward (Wang et al., 2020; Xie et al., 2020). RH, however, exhibits a more complex pattern, with positive SHAP values occurring across both low- and high-RH conditions, reflecting the strong condition dependence of RH contributions. Finally, as the least influential factor, PM_1 mass loading also contributes positively to aerosol pH, with higher PM_1 concentration being associated with larger SHAP values.

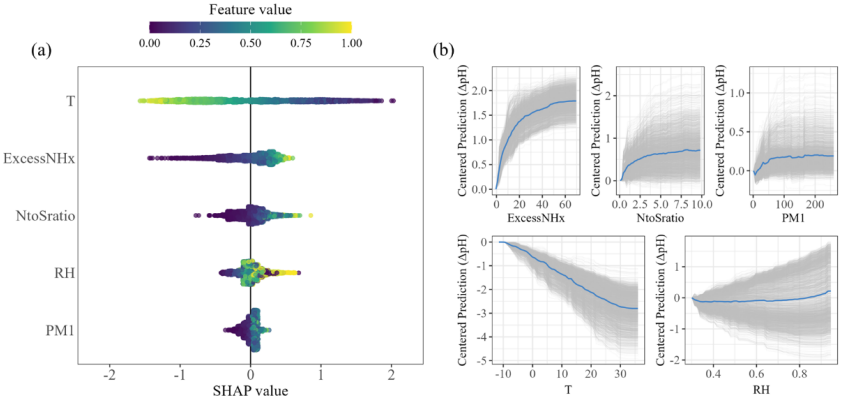

Figure 2. Global SHAP summary plot showing the relative importance and overall contributions of individual features, including temperature (T, °C), Excess NHx (μg m^{-3}), nitrate-to-sulfate mass ratio (NtoSratio), PM_1 mass loading (μg m^{-3}), and RH, to aerosol pH (a), and c-ICE curves illustrating sample-specific effects of each feature on aerosol pH (gray lines) along with their averaged responses (blue line) (b).

The c-ICE analysis further resolves variable-specific responses (Fig. 2b). For temperature, Excess NHx, N/S ratio, and PM_1 mass, c-ICE curves generally align with global SHAP trends, indicating their largely monotonic influences on predicted pH across samples. In particular, the average decreasing trend of pH with temperature corresponds to a reduction of ~0.6 units per 10 °C increase, consistent with the ISORROPIA II thermodynamic sensitivity test results (Fig. S4). For Excess NHx, increases at lower concentrations correspond to substantial rises in predicted pH, with a 20 μg m^{-3} increase associated with a nearly 1.5 units rise in pH, while the response flattens at higher concentrations, implying decreasing sensitivity (Liu et al., 2017;

https://doi.org/10.5194/egusphere-2026-1855
Preprint. Discussion started: 17 April 2026
© Author(s) 2026. CC BY 4.0 License.

Ding et al., 2019). RH, in contrast, exhibits markedly different behavior. The c-ICE curves reveal pronounced sample-to-sample variability, with approximately half of the samples showing positive pH responses to increasing RH and the remaining samples showing negative responses. This pronounced heterogeneity indicates that the RH contributions are highly condition-dependent, strongly modulated by interactions with other variables, which may be overlooked by traditional sensitivity tests based on average conditions (Fig. S4) and warrants further investigation.

3.2 Regime-dependent RH interactions with other factors

Pairwise interactions (Lundberg et al., 2020; Hou et al., 2022; Qi et al., 2025) between meteorological and chemical factors were analyzed to assess their combined contributions to pH prediction (Fig. 3 and Fig. S5). RH-related interactions are generally stronger and more systematical than those of other variable pairs, consistent with the pronounced condition-dependent c-ICE behavior of RH discussed above.

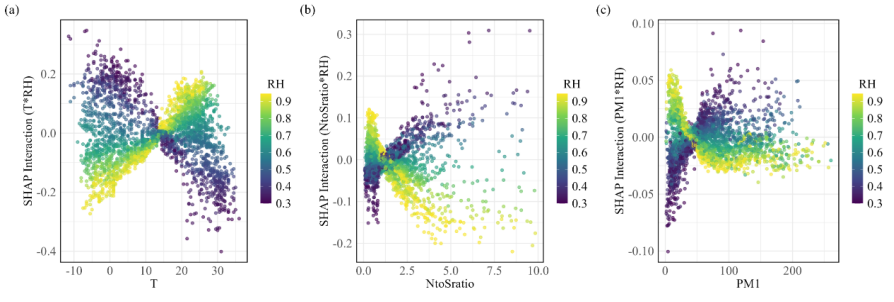

Figure 3. SHAP interaction plots illustrating the joint effects of RH with temperature (°C) (a), N/S mass ratio (b), and PM_1 mass loading (μg m^{-3}) (c) on aerosol pH prediction. The color scale represents RH, and the SHAP interaction values indicate the direction and magnitude of RH modulation on predicted pH under different regimes.

As two key meteorological parameters, temperature and RH exhibit strong statistical interactions in pH prediction, with opposite patterns across different regimes (Fig. 3a). The thresholds were identified from inflection points in the SHAP interaction plots. At temperatures below 15 °C, higher RH is associated with lower pH values in the model prediction at a given temperature, with RH–temperature interaction SHAP values showing a maximum decrease

https://doi.org/10.5194/egusphere-2026-1855
Preprint. Discussion started: 17 April 2026
© Author(s) 2026. CC BY 4.0 License.

from approximately 0.30 to −0.25. In contrast, at temperatures above 15 °C, this interaction reverses, with higher RH corresponding to higher predicted pH. Specifically, higher predicted aerosol acidity occurs under both low-temperature–high-RH and high-temperature–low-RH conditions, whereas the opposite combinations correspond to lower acidity.

This regime-dependent behavior can be explained by the coupled influence of temperature and RH on secondary inorganics formation, gas–particle partitioning and aerosol water uptake, which together modulate the balance between H^+ input and dilution (Ding et al., 2019; Tao et al., 2025). Under low-temperature conditions, thermodynamic equilibrium favors the partitioning of semi-volatile species into the particle phase (Guo et al., 2015). Elevated RH could not only increase ALWC but also facilitate heterogeneous reactions of gaseous precursors to form secondary inorganic aerosols, accompanied by H^+ accumulation (Liu et al., 2017; Ding et al., 2019). As shown in Fig. 4, at temperatures below 15 °C, both H^+ and ALWC increased with RH, accompanied by a decrease in pH. That means under low-temperature conditions, enhanced inorganic aerosol formation and associated H^+ accumulation likely outweigh the concurrent increase in ALWC and its dilution effect, resulting in increased aerosol acidity. In contrast, at higher temperatures, enhanced volatilization shifts gas-particle partitioning towards the gas phase, likely limiting H^+ accumulation in particles (Ding et al., 2019; Tao et al., 2025). Consistently, at temperatures above 15 °C, H^+ slightly decreased with increasing RH, while ALWC continued to increase and pH correspondingly increased (Fig. 4). In this regime, the dominant effect of higher RH should be the enhancement of ALWC dilution, resulting in lower aerosol acidity. Temperature therefore modulates whether RH-driven H^+ accumulation or ALWC dilution prevails, producing opposite RH sensitivities across different regimes.

https://doi.org/10.5194/egusphere-2026-1855
Preprint. Discussion started: 17 April 2026
© Author(s) 2026. CC BY 4.0 License.

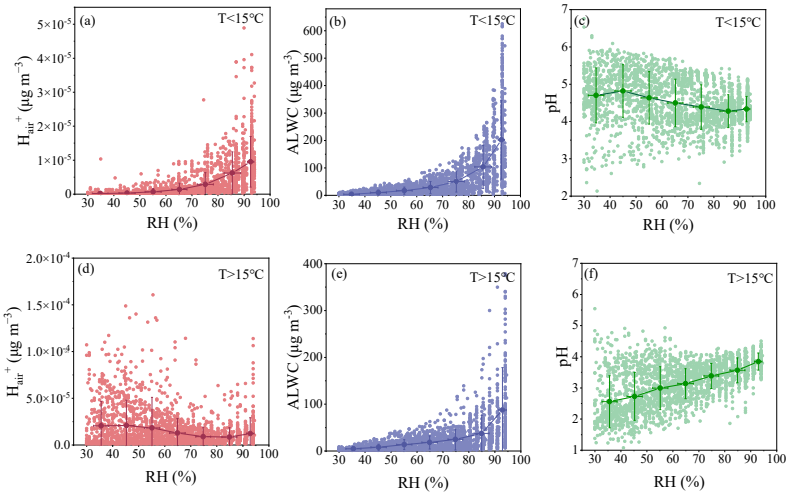

Figure 4. Scatter plots of H_{air}^+ (μg m^{-3}), ALWC (μg m^{-3}), and pH versus RH, along with their average variation trends with RH for temperature lower than 15℃ (a, b, c), and higher than 15℃ (d, e, f), respectively.

Strong statistical interactions were also observed between RH and chemical parameters, including the N/S ratio and PM_1 mass loading, both exhibiting clear threshold-dependent regime shifts (Fig. 3b, c). Under sulfate-dominant conditions (N/S ratio < ~1.25), higher RH tends to be associated with higher predicted pH, whereas this pattern reverses under nitrate-dominant conditions (N/S ratio > ~1.25), where higher RH is associated with lower predicted pH. A similar regime-dependent behavior is evident for PM_1 mass loading, with RH exerting a positive contribution to predicted pH at low PM_1 concentrations (< 50 μg m^{-3}) but an increasingly negative contribution at higher loadings (> 50 μg m^{-3}). Consistently, under sulfate-dominant or low-mass conditions (N/S < 1.25 or PM_1 < 50 μg m^{-3}), H^+ slightly decreased while ALWC continued to increase with increasing RH, such that dilution by aerosol water likely outweighed, resulting in elevated pH (Fig. 5). In contrast, under nitrate-dominant or high-mass conditions (N/S > 1.25 or PM_1 > 50 μg m^{-3}), concurrent enhancements in both H^+ and ALWC were observed with increasing RH, accompanied by a slight decrease in pH, reflecting that H^+ accumulation likely outweighed the concurrent dilution by ALWC.

https://doi.org/10.5194/egusphere-2026-1855
Preprint. Discussion started: 17 April 2026
© Author(s) 2026. CC BY 4.0 License.

These might be related to the complex multiphase chemical processes among different regimes. Under cleaner periods with low PM_1 loading, elevated RH substantially increases ALWC while secondary inorganic aerosol formation remains relatively limited due to lower precursor concentrations. Consequently, the dilution effect likely dominates, resulting in increased pH. In contrast, under higher PM_1 loading, abundant particles provide extensive reaction media, and enhanced water uptake at high RH could facilitate heterogeneous/aqueous-phase formation of secondary inorganic aerosols (Wang et al., 2025). The resulting H^+ accumulation likely outweighs the water dilution effect and decreases pH (Fig. 5). Regarding the RH–N/S interaction, NH_3 first neutralizes sulfuric acid and subsequently reacts with HNO_3, and aerosol pH generally decreases with increasing sulfate but increases with increasing nitrate (Ding et al., 2019; Xie et al., 2020). Under sulfate-dominant conditions (low N/S), increased RH enhances the aqueous uptake of NH_3, partially neutralizing existing acidity and mainly promoting the formation of NH_4NO_3 (Fig. S6), which is therefore likely associated with an increase in pH. In contrast, under nitrate-dominant conditions (high N/S), the increase in sulfate mass with RH is more pronounced than that of nitrate (Fig. S6). That means under this regime, the efficient aqueous medium is likely more favorable for sulfate production (e.g., through multiphase oxidation of SO_2 and NO_x) (Wang et al., 2016). This process likely introduces additional acidity to the particle phase and leads to a decrease in pH again. These results underscore the importance of multiphase chemical processes in influencing aerosol pH variation under different environmental regimes.

https://doi.org/10.5194/egusphere-2026-1855
Preprint. Discussion started: 17 April 2026
© Author(s) 2026. CC BY 4.0 License.

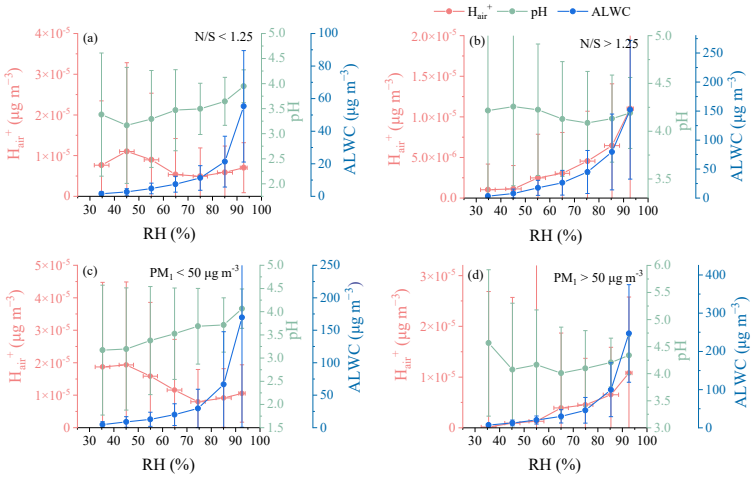

Figure 5. Variations of H_{air}^+ (μg m^{-3}), ALWC (μg m^{-3}), and pH as a function of RH under different environmental conditions: (a) N/S mass ratio < 1.25, (b) N/S mass ratio > 1.25, separated by the nitrate-to-sulfate mass ratio; (c) PM_1 mass loading < 50 μg m^{-3}, and (d) PM_1 mass loading > 50 μg m^{-3}, separated by PM_1 mass loading levels.

3.3 Seasonal patterns of RH-associated variability in aerosol pH

The regime-dependent relationship between aerosol pH and RH identified by SHAP provides a coherent framework for interpreting the seasonal patterns observed during our ammonia-rich campaign. For example, RH generally showed negative contributions to pH in winter, whereas in summer it exerted a positive association with pH and ranked as the largest contributor to pH variability (Fig. 6). This seasonal reversal aligns with the RH–temperature/chemical interactions discussed above. Low winter temperatures (<10 °C) place pH within regimes where elevated RH is linked to higher aerosol acidity, whereas higher summer temperatures (12–40 °C) shift pH into regimes where higher RH is associated with lower acidity (Fig. S7). In addition, lower PM_1 mass loadings in summer (with a peak frequency at ~30 μg m^{-3}) compared to winter (with a peak frequency at ~90 μg m^{-3}) align with the positive RH–pH relationship under low PM_1 conditions and the negative relationship under high PM_1 conditions discussed above (Fig. S7). Such seasonally contrasting RH–pH associations also agree with thermodynamic sensitivity analyses conducted by Ding et al. (2019), reinforcing the plausibility of the

https://doi.org/10.5194/egusphere-2026-1855
Preprint. Discussion started: 17 April 2026
© Author(s) 2026. CC BY 4.0 License.

interaction patterns identified here. Overall, these results highlight that RH-related pH variability should be interpreted in conjunction with temperature and the prevailing chemical buffering regime.

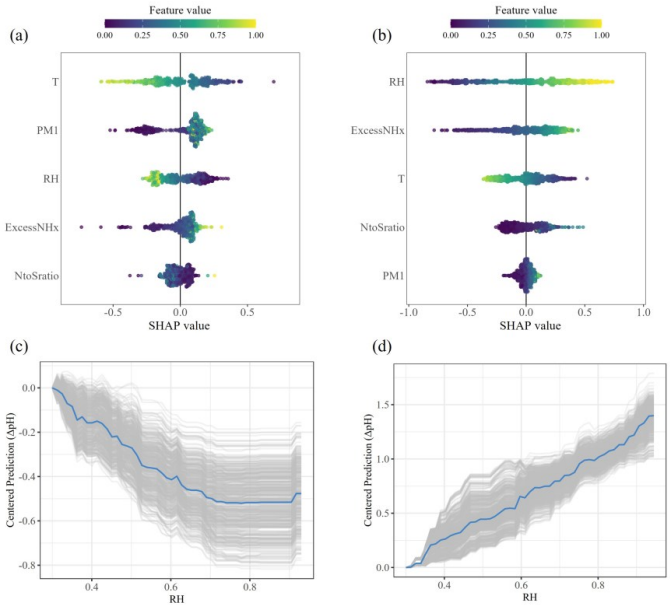

Figure 6. SHAP values showing the relative importance of input features for aerosol pH during the winter (a) and summer (b) periods, illustrating their contributions to pH variability. c-ICE curves (gray lines) and their averages (blue line) depicting the relationships between RH and pH between winter (c) and summer (d).

4. Conclusions and implications

In this study, we provide a comprehensive, data-driven assessment of aerosol pH variability in an ammonia-rich urban atmosphere by integrating machine learning, field observations, and thermodynamic modeling. Our results indicate that aerosol pH is closely associated with both meteorological conditions and chemical composition. Temperature shows a dominant negative contribution, whereas excess ammonia, N/S ratio, and PM_1 mass loading are positively associated with pH. The contribution of RH, however, is highly regime-dependent, with its contribution reversing under different combinations of temperature, chemical composition, and

https://doi.org/10.5194/egusphere-2026-1855
Preprint. Discussion started: 17 April 2026
© Author(s) 2026. CC BY 4.0 License.

aerosol loading. By quantifying threshold boundaries, visualizing regime transitions, and resolving sample-level variability, the SHAP framework complements traditional thermodynamic analyses and provides quantitative insights into the conditions under which RH is linked to higher or lower aerosol pH.

The thresholds and interaction patterns identified here are based on observations at a single urban site in Beijing and may therefore reflect local meteorology and emission characteristics. Nevertheless, this approach provides a quantitative framework for understanding and predicting aerosol pH responses under evolving atmospheric environments. In China's increasingly ammonia-rich atmosphere, aerosol pH response generally falls within a flattened regime, exhibiting weak sensitivity to further increases in ammonia. Under such conditions, meteorological factors, together with particle properties such as total mass loading and the relative contributions of sulfate and nitrate, will jointly modulate aerosol acidity. Ongoing decreases in particle mass and the gradual shift from sulfate-dominated to nitrate-dominated composition in recent years are expected to substantially modify aerosol buffering properties. Additionally, distinct environment conditions not considered in this study, such as coastal regions influenced by sea salt (Wang et al., 2022; Xu et al., 2025) and dust-affected areas enriched in alkaline metals (Shi et al., 2019; Huang et al., 2020), may also exert important roles in pH variation. Extending this SHAP-based analytical framework to diverse atmospheric conditions will enable a more general characterization of pH regimes in ammonia-rich environments and improve predictive capability under a wide range of future scenarios.

Data availability. The data used in this study can be obtained from https://doi.org/10.5281/zenodo.19585092 (Duan and Wang, 2026). It is also available from the corresponding author upon request.

Author contributions. RJH designed the study. JD and TW performed the data analysis and interpretation, with contributions from JYR, HBZ, and WX. JD, TW and RJH wrote the manuscript, and all authors contributed to scientific discussions and revision of the manuscript.

Competing interests. The authors declare that they have no conflict of interest.

https://doi.org/10.5194/egusphere-2026-1855
Preprint. Discussion started: 17 April 2026
© Author(s) 2026. CC BY 4.0 License.

Acknowledgements. This work was supported by the National Natural Science Foundation of China (NSFC) (grant no. 42525301, 42430708, and 42577125), the Key Research Program of Frontier Sciences from the Chinese Academy of Sciences (ZDBS-LY-DQC001), the Innovation Capability Support Program of Shaanxi (2024RS-CXTD-40), and the New Cornerstone Science Foundation through the XPLORER PRIZE.

Reference

Battaglia Jr, M. A., Weber, R. J., Nenes, A., and Hennigan, C. J.: Effects of water-soluble organic carbon on aerosol pH, Atmos. Chem. Phys., 19, 14607-14620, 10.5194/acp-19-14607-2019, 2019.

Cai, A., Wang, L., Zhang, Y., Wu, H., Zhang, H., Guo, R., and Wu, J.: Uncovering the multiple socio-economic driving factors of carbon emissions in nine urban agglomerations of China based on machine learning, Energy, 319, 134859, 10.1016/j.energy.2025.134859, 2025.

Cao, Y., Zhang, Z., Xiao, H., Xie, Y., Liang, Y., and Xiao, H.: How aerosol pH responds to nitrate to sulfate ratio of fine-mode particulate, Environ Sci Pollut Res Int, 27, 35031-35039, 10.1007/s11356-020-09810-0, 2020.

Clegg, S. L., Seinfeld, J. H., and Brimblecombe, P.: Thermodynamic modelling of aqueous aerosols containing electrolytes and dissolved organic compounds, Journal of aerosol science, 32, 713-738, 2001.

Dai, T., Dai, Q., Ding, J., Liu, B., Bi, X., Wu, J., Zhang, Y., and Feng, Y.: Measuring the Emission Changes and Meteorological Dependence of Source-Specific BC Aerosol Using Factor Analysis Coupled With Machine Learning, J. Geophys. Res.-Atmos., 128, e2023JD038696, 10.1029/2023jd038696, 2023.

Ding, J., Zhao, P., Su, J., Dong, Q., Du, X., and Zhang, Y.: Aerosol pH and its driving factors in Beijing, Atmos. Chem. Phys., 19, 7939-7954, 10.5194/acp-19-7939-2019, 2019.

Duan, X., Zheng, G., Chen, C., Zhang, Q., and He, K.: Driving factors of aerosol acidity: a new hierarchical quantitative analysis framework and its application in Changzhou, China, Atmos. Chem. Phys., 25, 3919-3928, 10.5194/acp-25-3919-2025, 2025.

Fountoukis, C. and Nenes, A.: ISORROPIA II: a computationally efficient thermodynamic equilibrium model for K^+–Ca^{2+}–Mg^{2+}–NH_4^+–Na^+–SO_4^{2-}–NO_3^-–Cl^-–H_2O aerosols, Atmos.

https://doi.org/10.5194/egusphere-2026-1855
Preprint. Discussion started: 17 April 2026
© Author(s) 2026. CC BY 4.0 License.

Chem. Phys., 7, 4639-4659, 2007.

Fu, Z., Cheng, L., Ye, X., Ma, Z., Wang, R., Duan, Y., Juntao, H., and Chen, J.: Characteristics of aerosol chemistry and acidity in Shanghai after PM(2.5) satisfied national guideline: Insight into future emission control, Sci. Total Environ., 827, 154319, 10.1016/j.scitotenv.2022.154319, 2022.

Giorio, C., D'Aronco, S., Di Marco, V., Badocco, D., Battaglia, F., Solda, L., Pastore, P., and Tapparo, A.: Emerging investigator series: aqueous-phase processing of atmospheric aerosol influences dissolution kinetics of metal ions in an urban background site in the Po Valley, Environ. Sci.: Process. Impacts, 24, 884-897, 10.1039/d2em00023g, 2022.

Grange, S. K., Carslaw, D. C., Lewis, A. C., Boleti, E., and Hueglin, C.: Random forest meteorological normalisation models for Swiss PM10 trend analysis, Atmos. Chem. Phys., 18, 6223-6239, 10.5194/acp-18-6223-2018, 2018.

Gui, K., Che, H., Zeng, Z., Wang, Y., Zhai, S., Wang, Z., Luo, M., Zhang, L., Liao, T., Zhao, H., Li, L., Zheng, Y., and Zhang, X.: Construction of a virtual PM(2.5) observation network in China based on high-density surface meteorological observations using the Extreme Gradient Boosting model, Environ. Int., 141, 105801, 10.1016/j.envint.2020.105801, 2020.

Guo, H., Liu, J., Froyd, K. D., Roberts, J. M., Veres, P. R., Hayes, P. L., Jimenez, J. L., Nenes, A., and Weber, R. J.: Fine particle pH and gas–particle phase partitioning of inorganic species in Pasadena, California, during the 2010 CalNex campaign, Atmos. Chem. Phys., 17, 5703-5719, 10.5194/acp-17-5703-2017, 2017.

Guo, H., Sullivan, A. P., Campuzano-Jost, P., Schroder, J. C., Lopez-Hilfiker, F. D., Dibb, J. E., Jimenez, J. L., Thornton, J. A., Brown, S. S., Nenes, A., and Weber, R. J.: Fine particle pH and the partitioning of nitric acid during winter in the northeastern United States, J. Geophys. Res.-Atmos., 121, 10-355, 10.1002/2016jd025311, 2016.

Guo, H., Xu, L., Bougiatioti, A., Cerully, K. M., Capps, S. L., Hite, J. R., Carlton, A. G., Lee, S. H., Bergin, M. H., Ng, N. L., Nenes, A., and Weber, R. J.: Fine-particle water and pH in the southeastern United States, Atmos. Chem. Phys., 15, 5211-5228, 10.5194/acp-15-5211-2015, 2015.

https://doi.org/10.5194/egusphere-2026-1855
Preprint. Discussion started: 17 April 2026
© Author(s) 2026. CC BY 4.0 License.

411 Hennigan, C. J., Izumi, J., Sullivan, A. P., Weber, R. J., and Nenes, A.: A critical evaluation of
412 proxy methods used to estimate the acidity of atmospheric particles, Atmos. Chem. Phys.,
413 15, 2775-2790, 10.5194/acp-15-2775-2015, 2015.
414 Hou, L., Dai, Q., Song, C., Liu, B., Guo, F., Dai, T., Li, L., Liu, B., Bi, X., Zhang, Y., and Feng,
415 Y.: Revealing Drivers of Haze Pollution by Explainable Machine Learning, Environ. Sci.
416 Technol. Lett., 9, 112-119, 10.1021/acs.estlett.1c00865, 2022.
417 Huang, R. J., Duan, J., Li, Y., Chen, Q., Chen, Y., Tang, M., Yang, L., Ni, H., Lin, C., Xu, W.,
418 Liu, Y., Chen, C., Yan, Z., Ovadnevaite, J., Ceburnis, D., Dusek, U., Cao, J., Hoffmann,
419 T., and O'Dowd, C. D.: Effects of NH(3) and alkaline metals on the formation of particulate
420 sulfate and nitrate in wintertime Beijing, Sci. Total Environ., 717, 137190,
421 10.1016/j.scitotenv.2020.137190, 2020.
422 Jia, S., Chen, W., Zhang, Q., Krishnan, P., Mao, J., Zhong, B., Huang, M., Fan, Q., Zhang, J.,
423 Chang, M., Yang, L., and Wang, X.: A quantitative analysis of the driving factors affecting
424 seasonal variation of aerosol pH in Guangzhou, China, Sci. Total Environ., 725, 138228,
425 10.1016/j.scitotenv.2020.138228, 2020.
426 Liu, M., Song, Y., Zhou, T., Xu, Z., Yan, C., Zheng, M., Wu, Z., Hu, M., Wu, Y., and Zhu, T.:
427 Fine particle pH during severe haze episodes in northern China, Geophys. Res. Lett., 44,
428 5213-5221, 10.1002/2017gl073210, 2017.
429 Lundberg, S. M., Erion, G., Chen, H., DeGrave, A., Prutkin, J. M., Nair, B., Katz, R.,
430 Himmelfarb, J., Bansal, N., and Lee, S. I.: From Local Explanations to Global
431 Understanding with Explainable AI for Trees, Nat. Mach. Intell., 2, 56-67,
432 10.1038/s42256-019-0138-9, 2020.
433 Maasikmets, M., Teinemaa, E., Kaasik, A., and Kimmel, V.: Measurement and analysis of
434 ammonia, hydrogen sulphide and odour emissions from the cattle farming in Estonia,
435 Biosyst. Eng., 139, 48-59, 10.1016/j.biosystemseng.2015.08.002, 2015.
436 Mo, Y., Li, J., Liu, J., Zhong, G., Cheng, Z., Tian, C., Chen, Y., and Zhang, G.: The influence
437 of solvent and pH on determination of the light absorption properties of water-soluble
438 brown carbon, Atmos. Environ., 161, 90-98, 10.1016/j.atmosenv.2017.04.037, 2017.
439 Myriokefalitakis, S., Ito, A., Kanakidou, M., Nenes, A., Krol, M. C., Mahowald, N. M., Scanza,

https://doi.org/10.5194/egusphere-2026-1855
Preprint. Discussion started: 17 April 2026
© Author(s) 2026. CC BY 4.0 License.

R. A., Hamilton, D. S., Johnson, M. S., Meskhidze, N., Kok, J. F., Guieu, C., Baker, A. R., Jickells, T. D., Sarin, M. M., Bikkina, S., Shelley, R., Bowie, A., Perron, M. M. G., and Duce, R. A.: Reviews and syntheses: the GESAMP atmospheric iron deposition model intercomparison study, Biogeosciences, 15, 6659-6684, 10.5194/bg-15-6659-2018, 2018.

Ng, N. L., Herndon, S. C., Trimborn, A., Canagaratna, M. R., Croteau, P. L., Onasch, T. B., Sueper, D., Worsnop, D. R., Zhang, Q., Sun, Y. L., and Jayne, J. T.: An Aerosol Chemical Speciation Monitor (ACSM) for Routine Monitoring of the Composition and Mass Concentrations of Ambient Aerosol, Aerosol. Sci. Tech., 45, 780-794, 10.1080/02786826.2011.560211, 2011.

Peng, X., Xie, T.-T., Tang, M.-X., Cheng, Y., Peng, Y., Wei, F.-H., Cao, L.-M., Yu, K., Du, K., He, L.-Y., and Huang, X.-F.: Critical Role of Secondary Organic Aerosol in Urban Atmospheric Visibility Improvement Identified by Machine Learning, Environ. Sci. Technol. Lett., 10, 976-982, 10.1021/acs.estlett.3c00084, 2023.

Qi, J., Xiong, W., Li, J., Zheng, J., Ye, Q., and Hu, M.: Investigating non-linear and synergistic effects of urban functional zone morphology on land surface temperature, Sustain. Cities Soc., 130, 106546, 10.1016/j.scs.2025.106546, 2025.

Qin, Y., Ye, J., Ohno, P., Liu, P., Wang, J., Fu, P., Zhou, L., Li, Y. J., Martin, S. T., and Chan, C. K.: Assessing the Nonlinear Effect of Atmospheric Variables on Primary and Oxygenated Organic Aerosol Concentration Using Machine Learning, ACS Earth Space Chem., 6, 1059-1066, 10.1021/acsearthspacechem.1c00443, 2022.

Sharma, B., Jia, S., Polana, A. J., Ahmed, M. S., Haque, R. R., Singh, S., Mao, J., and Sarkar, S.: Seasonal variations in aerosol acidity and its driving factors in the eastern Indo-Gangetic Plain: A quantitative analysis, Chemosphere, 305, 135490, 10.1016/j.chemosphere.2022.135490, 2022.

Shi, G., Xu, J., Shi, X., Liu, B., Bi, X., Xiao, Z., Chen, K., Wen, J., Dong, S., Tian, Y., Feng, Y., Yu, H., Song, S., Zhao, Q., Gao, J., and Russell, A. G.: Aerosol pH Dynamics During Haze Periods in an Urban Environment in China: Use of Detailed, Hourly, Speciated Observations to Study the Role of Ammonia Availability and Secondary Aerosol Formation and Urban Environment, J. Geophys. Res.-Atmos., 124, 9730-9742,

https://doi.org/10.5194/egusphere-2026-1855
Preprint. Discussion started: 17 April 2026
© Author(s) 2026. CC BY 4.0 License.

10.1029/2018jd029976, 2019.

Song, C., Becagli, S., Beddows, D. C. S., Brean, J., Browse, J., Dai, Q., Dall'Osto, M., Ferracci, V., Harrison, R. M., Harris, N., Li, W., Jones, A. E., Kirchgassner, A., Kramawijaya, A. G., Kurganskiy, A., Lupi, A., Mazzola, M., Severi, M., Traversi, R., and Shi, Z.: Understanding Sources and Drivers of Size-Resolved Aerosol in the High Arctic Islands of Svalbard Using a Receptor Model Coupled with Machine Learning, Environ. Sci. Technol., 56, 11189-11198, 10.1021/acs.est.1c07796, 2022.

Song, S., Gao, M., Xu, W., Shao, J., Shi, G., Wang, S., Wang, Y., Sun, Y., and McElroy, M. B.: Fine-particle pH for Beijing winter haze as inferred from different thermodynamic equilibrium models, Atmos. Chem. Phys., 18, 7423-7438, 10.5194/acp-18-7423-2018, 2018.

Su, H., Cheng, Y., and Poschl, U.: New Multiphase Chemical Processes Influencing Atmospheric Aerosols, Air Quality, and Climate in the Anthropocene, Acc. Chem. Res., 53, 2034-2043, 10.1021/acs.accounts.0c00246, 2020.

Tao, J., Wu, Y., Deng, Y., Hu, B., and Zhou, Z.: Thermodynamic regulation of aerosol pH by temperature and humidity: The role of gas-particle partitioning of semi-volatile inorganic species in a subtropical region, Environ. Res., 286, 122727, 10.1016/j.envres.2025.122727, 2025.

Tao, Y. and Murphy, J. G.: The Mechanisms Responsible for the Interactions among Oxalate, pH, and Fe Dissolution in PM2.5, ACS Earth Space Chem., 3, 2259-2265, 10.1021/acsearthspacechem.9b00172, 2019.

Tao, Y. and Murphy, J. G.: Simple Framework to Quantify the Contributions from Different Factors Influencing Aerosol pH Based on NH(x) Phase-Partitioning Equilibrium, Environ. Sci. Technol., 55, 10310-10319, 10.1021/acs.est.1c03103, 2021.

Tilgner, A., Schaefer, T., Alexander, B., Barth, M., Collett, J. L., Jr., Fahey, K. M., Nenes, A., Pye, H. O. T., Herrmann, H., and McNeill, V. F.: Acidity and the multiphase chemistry of atmospheric aqueous particles and clouds, Atmos. Chem. Phys., 21, 13483-13536, 10.5194/acp-21-13483-2021, 2021.

Wang, G., Tao, Y., Chen, J., Liu, C., Qin, X., Li, H., Yun, L., Zhang, M., Zheng, H., Gui, H.,

https://doi.org/10.5194/egusphere-2026-1855
Preprint. Discussion started: 17 April 2026
© Author(s) 2026. CC BY 4.0 License.

Liu, J., Huo, J., Fu, Q., Deng, C., and Huang, K.: Quantitative Decomposition of Influencing Factors to Aerosol pH Variation over the Coasts of the South China Sea, East China Sea, and Bohai Sea, Environ. Sci. Technol. Lett., 9, 815-821, 10.1021/acs.estlett.2c00527, 2022.

Wang, G., Zhang, R., Gomez, M. E., Yang, L., Levy Zamora, M., Hu, M., Lin, Y., Peng, J., Guo, S., Meng, J., Li, J., Cheng, C., Hu, T., Ren, Y., Wang, Y., Gao, J., Cao, J., An, Z., Zhou, W., Li, G., Wang, J., Tian, P., Marrero-Ortiz, W., Secrest, J., Du, Z., Zheng, J., Shang, D., Zeng, L., Shao, M., Wang, W., Huang, Y., Wang, Y., Zhu, Y., Li, Y., Hu, J., Pan, B., Cai, L., Cheng, Y., Ji, Y., Zhang, F., Rosenfeld, D., Liss, P. S., Duce, R. A., Kolb, C. E., and Molina, M. J.: Persistent sulfate formation from London Fog to Chinese haze, Proc Natl Acad Sci U S A, 113, 13630-13635, 10.1073/pnas.1616540113, 2016.

Wang, J., Wu, Z., Qiu, T., Man, R., Zong, T., Qiu, Y., Fang, W., Chen, S., Liang, D., Song, M., Ahn, J., Lee, J., and Hu, M.: Impacts of aerosol acidity and liquid water content on secondary inorganic aerosol pollution in East Asian megacities: Beijing and Seoul, Atmos. Environ., 361, 10.1016/j.atmosenv.2025.121479, 2025.

Wang, S., Wang, L., Li, Y., Wang, C., Wang, W., Yin, S., and Zhang, R.: Effect of ammonia on fine-particle pH in agricultural regions of China: comparison between urban and rural sites, Atmos. Chem. Phys., 20, 2719-2734, 10.5194/acp-20-2719-2020, 2020.

Wang, Y. C., Huang, R. J., Ni, H. Y., Chen, Y., Wang, Q. Y., Li, G. H., Tie, X. X., Shen, Z. X., Huang, Y., Liu, S. X., Dong, W. M., Xue, P., Fröhlich, R., Canonaco, F., Elser, M., Daellenbach, K. R., Bozzetti, C., El Haddad, I., Prévôt, A. S. H., Canagaratna, M. R., Worsnop, D. R., and Cao, J. J.: Chemical composition, sources and secondary processes of aerosols in Baoji city of northwest China, Atmos. Environ., 158, 128-137, 10.1016/j.atmosenv.2017.03.026, 2017.

Wei, N., Jia, Z., Men, Z., Ren, C., Zhang, Y., Peng, J., Wu, L., Wang, T., Zhang, Q., and Mao, H.: Machine Learning Predicts Emissions of Brake Wear PM2.5: Model Construction and Interpretation, Environ. Sci. Technol. Lett., 9, 352-358, 10.1021/acs.estlett.2c00117, 2022.

Wei, Y., Wang, S., Jiang, N., Zhang, R., and Hao, Q.: Comparative multi-model study of PM(2.5) acidity trend changes in ammonia-rich regions in winter: Based on a new ammonia

https://doi.org/10.5194/egusphere-2026-1855
Preprint. Discussion started: 17 April 2026
© Author(s) 2026. CC BY 4.0 License.

concentration assessment method, J. Hazard. Mater., 458, 131970, 10.1016/j.jhazmat.2023.131970, 2023.

Xie, F., Su, Y., Tian, Y., Shi, Y., Zhou, X., Wang, P., Yu, R., Wang, W., He, J., Xin, J., and Lü, C.: The shifting of secondary inorganic aerosol formation mechanisms during haze aggravation: the decisive role of aerosol liquid water, Atmos. Chem. Phys., 23, 2365-2378, 10.5194/acp-23-2365-2023, 2023.

Xie, Y., Wang, G., Wang, X., Chen, J., Chen, Y., Tang, G., Wang, L., Ge, S., Xue, G., Wang, Y., and Gao, J.: Nitrate-dominated PM2.5 and elevation of particle pH observed in urban Beijing during the winter of 2017, Atmos. Chem. Phys., 20, 5019-5033, 10.5194/acp-20-5019-2020, 2020.

Xu, K., Yin, L., Chen, Q., Liao, D., Ji, X., Zhang, K., Wu, Y., Xu, L., Li, M., Fan, X., Zhang, F., Huang, Z., Chen, J., and Hong, Y.: Quantitative analysis of influencing factors to aerosol pH and its responses to PM(2.5) and O(3) pollution in a coastal city, J. Environ. Sci., 151, 284-297, 10.1016/j.jes.2024.03.044, 2025.

Yang, C., Dong, H., Chen, Y., Wang, Y., Fan, X., Tham, Y. J., Chen, G., Xu, L., Lin, Z., Li, M., Hong, Y., and Chen, J.: Machine Learning Reveals the Parameters Affecting the Gaseous Sulfuric Acid Distribution in a Coastal City: Model Construction and Interpretation, Environ. Sci. Technol. Lett., 10, 1045-1051, 10.1021/acs.estlett.3c00170, 2023.

Yang, C., Dong, H., Chen, Y., Xu, L., Chen, G., Fan, X., Wang, Y., Tham, Y. J., Lin, Z., Li, M., Hong, Y., and Chen, J.: New Insights on the Formation of Nucleation Mode Particles in a Coastal City Based on a Machine Learning Approach, Environ. Sci. Technol., 58, 1187-1198, 10.1021/acs.est.3c07042, 2024.

Yang, J., Wang, S., Zhang, R., and Yin, S.: Elevated particle acidity enhanced the sulfate formation during the COVID-19 pandemic in Zhengzhou, China, Environ. Pollut., 296, 118716, 10.1016/j.envpol.2021.118716, 2022.

Zhang, B., Shen, H., Liu, P., Guo, H., Hu, Y., Chen, Y., Xie, S., Xi, Z., Skipper, T. N., and Russell, A. G.: Significant contrasts in aerosol acidity between China and the United States, Atmos. Chem. Phys., 21, 8341-8356, 10.5194/acp-21-8341-2021, 2021.

Zheng, G., Su, H., Wang, S., Andreae, M. O., Pöschl, U., and Cheng, Y.: Multiphase buffer

https://doi.org/10.5194/egusphere-2026-1855
Preprint. Discussion started: 17 April 2026
© Author(s) 2026. CC BY 4.0 License.

theory explains contrasts in atmospheric aerosol acidity, Science, 369, 1374-1377, 2020.

Zhou, M., Zheng, G., Wang, H., Qiao, L., Zhu, S., Huang, D., An, J., Lou, S., Tao, S., Wang, Q., Yan, R., Ma, Y., Chen, C., Cheng, Y., Su, H., and Huang, C.: Long-term trends and drivers of aerosol pH in eastern China, Atmos. Chem. Phys., 22, 13833-13844, 10.5194/acp-22-13833-2022, 2022.